Journal of the Korean Magnetic Resonance Society **2020**, *24*, 1-8
DOI 10.6564/JKMRS.2020.24.1.001

Backbone NMR assignments of the FAS1-3/FAS1-4 domains of transforming growth factor-beta-induced protein

Dong-Hoon Kang[1, ξ], Jong-Jae Yi[2, ξ], Dae-Won Sim[3], Jung-Wook Park[1], Sung-Hee Lee[1], Eun-Hee Kim[4], Young-Ho Jeon[5], Woo Sung Son[2], Hyung-Sik Won[3,*], and Ji-Hun Kim[1,*]

[1]College of Pharmacy, Chungbuk National University, Cheongju, Chungbuk 28160, Republic of Korea
[2]Department of Pharmacy, College of Pharmacy and Institute of Pharmaceutical Sciences, CHA University, Pochen, Gyeonggi 11160, Republic of Korea
[3]Department of Biotechnology, College of Biomedical and Health Science, Konkuk University, Chungju, Chungbuk 27478, Republic of Korea
[4]Research Center for Bioconvergence Analysis, Korea Basic Science Institute, 162 Yeongudanji-Ro, Ochang-Eup, Cheongju-Si, Chungcheongbuk-Do 28119, Republic of Korea
[5]Korea University College of Pharmacy Sejong-ro, Jochiwon, Yeonggi-gun, Chungnam 339-700, Republic of Korea

Received March 9, 2020; Revised March 15, 2020; Accepted March 16, 2020

Abstract An extracellular matrix protein, transforming growth factor-beta-induced protein (TGFBIp/βig-h3), which is induced by transforming growth factor-β in the human cornea, skin, and matrix of many connective tissues, is associated with the adhesion, migration, proliferation, and differentiation of various cells. TGFBIp contains four homologous repeat domains, known as FAS1 domains, where certain mutations have been considered to cause corneal dystrophies. In this study, backbone NMR assignments of FAS1-3/FAS1-4 tandem domain were obtained and compared with those previously known for the isolated FAS1-4 domain. The results corroborate in solution the inter-domain interaction between FAS1-3 and FAS1-4 in TGFBIp.

Keywords Blvrb, dialysis using micro-dialyzer, 1-dimensional HSQC experiment, ^{15}N-labeled protein, protein refolding

Introduction

Human transforming growth factor β-induced protein (TGFBIp), composed of 683 amino acid residues, was first identified through the analysis of gene expression induced by transforming growth factor β in cancer cell lines.[1] It is found ubiquitously in the extracellular matrix (ECM) of the various tissues and organ systems such as cornea, skin, bone, tendon endometrium, and kidney.[2-4] It is also found in the circulation, at ~300 ng/ml and in platelets.[5] The biological key role of TGFBIp has not been understood clearly, however, TGFBIp is known to play important roles in physiologic and pathologic responses such as wound healing, angiogenesis and inflammatory diseases by mediating cell adhesion.[3] It has been also reported that abnormal accumulation and stroma of insoluble mutated TGFBIp as amorphous and/or amylogenic form are related to TGFBIp-associated corneal dystrophies (CDs).[4, 6]

TGFBIp contains a secretory signal peptide sequence, a cysteine-rich EMI domain, four homologous Fas1 domains and a classic integrin-recognition motif (RGD, residues R^{642}-D^{644}).[7] The FAS1 domain represents a cell adhesion domain homologous to fasciclin I protein in *Drosophila* and mutations of several residues in these domains cause TGFBIp-

*Address correspondence to: **Ji-Hun Kim and Hyung-Sik Won**, College of Pharmacy, Chungbuk National University, Cheongju, Chungbuk 28160, Republic of Korea, Tel.: +82 43 249 1343; Email: nmrjhkim@cbnu.ac.kr / [3]Department of Biotechnology, College of Biomedical and Health Science, Konkuk University, Chungju, Chungbuk 27478, Republic of Korea, Tel: +82 43 840 3589; E-mail: wonhs@konkuk.ac.kr, ξ Equally contributed to this work

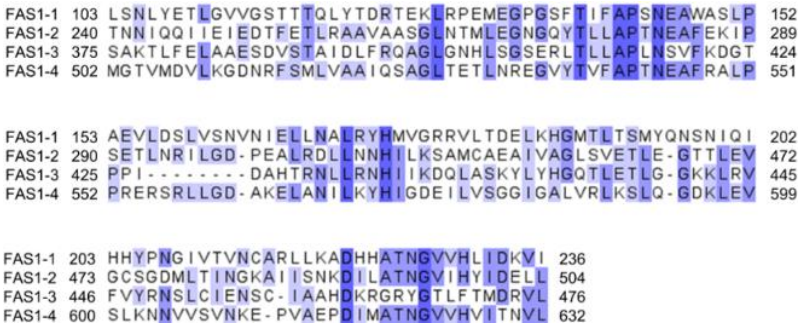

Figure 1. Identify-based sequence alignment of FAS1 domains in TGFBIp

CDs.[8, 9] In order to understand its function clearly, structure-based analyses with atomic resolution are essential. So far, most of structural studies have been conducted on the isolated FAS1-4 domain.[10-12] Recently, a crystal structure containing four FAS1 domains was reported.[3] Crystal structure describes that FAS1 domains are sandwiches of two perpendicular four-stranded β sheets decorated with two three-helix insertions, and adjacent domains FAS1-1/FAS1-2 and FAS1-3/FAS1-4 tightly interact in an equivalent manner. However, crystal structure is not frequently enough to explain structure-dynamics-function linkage. In order to fill this inadequate aspect, NMR is open used. Given the facts that integrin binding residues and the dystrophic mutations are found at FAS1-4 and FAS1-4 is strongly linked to FAS1-3, NMR studies on FAS1-3/FAS1-4 is essential to elucidate exact mechanism of TGFBIp at an atomic resolution.

Experimental Methods

Cloning and Plasmid Construction – A DNA plasmid of full length TGFBIp was provided from Kim and colleagues affiliated in department of biochemistry, school of medicine, Kyungpook National University.

The cDNAs of FAS1-3/FAS1-4 and FAS1-4 domain of TGFBIp, respectively, was amplified by polymerase chain reaction (PCR), and the cDNA was ligated into a pET15b vector using two restriction endonuclease sites, *NdeI* and *XhoI*. Final constructs contain N-terminal poly-histidine purification tag, MGHHHHHHG-, to facilitate efficient purification.

Recombinant expression of FAS1 domains of TGFBIp in E. coli – The vectors containing cDNA of FAS1-3/FAS1-4 and FAS1-4, respectively, were transformed into *E. coli* BL21(DE3) pLysS (Novagen), which produces T7 lysozyme to reduce basal level expression of the gene of interest. The product of the transformed culture was plated on LB-agar containing antibiotic resistances, ampicillin and chloramphenicol, before overnight incubation at 37 °C. A single colony from a freshly streaked plate was used to inoculate a starter culture with 5 ml of LB media and incubate at 37 °C for approximately 8 hours. A starter culture was transferred to a large flask with M9 media containing ampicillin, chloramphenicol, 0.1 mM $CaCl_2$, 1 mM $MgSO_4$, 1 g/L ^{15}N-ammonium chloride and 1 g/L ^{13}C-glucose for isotope labeling. Protein expression was induced with the addition of 1 mM IPTG when the OD_{600} reached 0.6. Following 8 hours of induction the cells were harvested by centrifugation.

Purification of FAS1 domains of TGFBIp – Harvested cells were resuspended in 100 mL of lysis buffer (20 mM Tris-HCl buffer, pH 7.3, 100 mM NaCl, and 20 mM imidazole and 0.2 ml of phenylmethylsulfonyl fluoride). Cell suspensions were lysed by sonication, and supernatants were collected by centrifugation at 15000 rpm for 30 min. Subsequently, supernatants were loaded onto nickel-affinity resin and the resin was washed with washing buffer containing 70 mM imidazole. FAS1 domains of TGFBIp were eluted

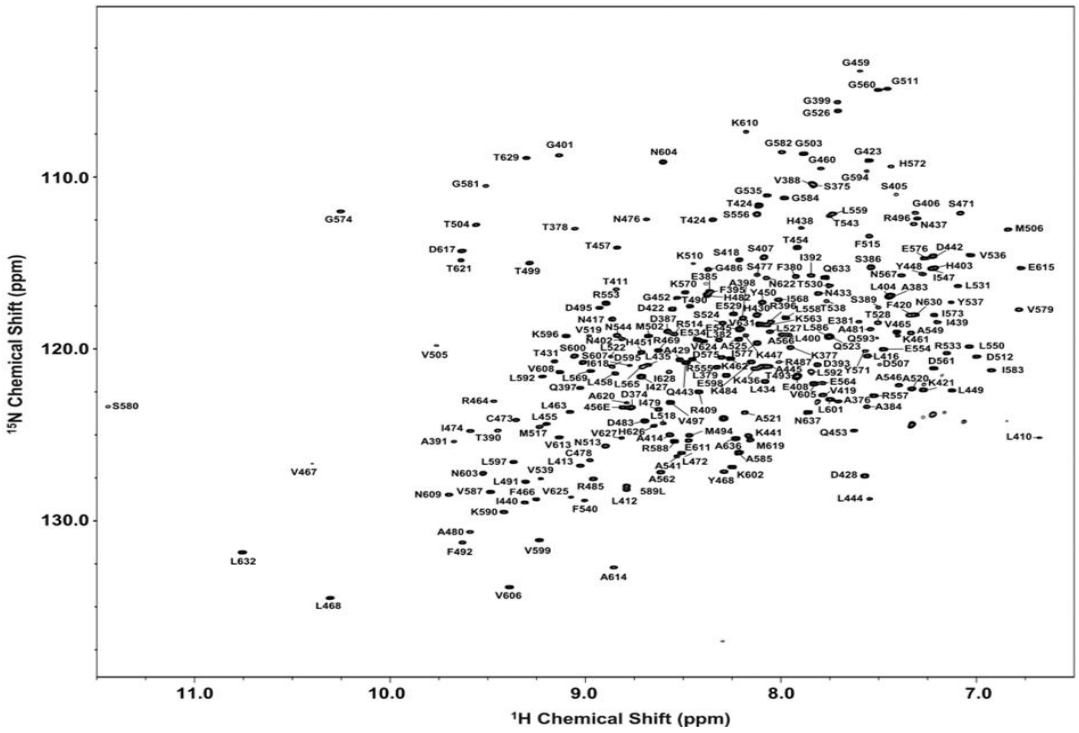

Figure 2. Assigned ^{1}H-^{15}N TROSY-HSQC spectrum of FAS1-3/FAS1-4. The spectrum was recorded in 900 MHz NMR spectrometer in 20 mM Tris- HCl containing 100 mM NaCl, at pH 7.3

using imidazole gradient manner, from 70 mM to 1 M imidazole. Next, the eluted FAS1 domains were digested by human thrombin at 22 °C, and followed by the removal of thrombin and other impurities via the sequential applications of Q-FF anion-exchange, and gel-permeation chromatography. The eluted proteins were buffer-exchanged to final buffer (20 mM Tris-HCl containing 100 mM NaCl, at pH 7.3) and concentrated at 4 °C using a centrifugal concentrator (10 kDa Amicon Ultra, EMD Millipore). The final concentration of protein was determined by using the extinction coefficient at 280 nm that was predicted by using sequence information.

NMR spectroscopy – All NMR spectra were measured using Bruker 800, 900 MHz NMR spectrometers equipped with TXI cryoprobes at 25 °C. NMR data were processed with NMRPipe, and analyzed with NMRView software. The chemical shifts of data were referenced directly to DSS for the ^{1}H atoms and indirectly for the ^{13}C and ^{15}N, using the chemical shift ratio value suggested in the BMRB (http://www.bmrb.wisc.edu). In order to complete assignment of backbone atoms, 3-dimenstional (3D) spectra such as HNCACB, HN(CO)CACB, HN(CA)CO and HNCO were measured.

Results and discussion

Sequence comparison of FAS1 domains – TGFBIp contains repeated four FAS1 domains, however, the sequence homology is not high, since the identities are only 18-33 % (figure 1). Whereas, according to reported crystal structure (PDB ID 5NV6), the four domains have high structural similarities with high root-mean-square deviation values of 1.4-3.3 Å. Secondary structure of FAS domains are similar but not same each other. For example, FAS1-1 contains additional helix (res. 182-187) and FAS1-3 lacks a helix.[13]

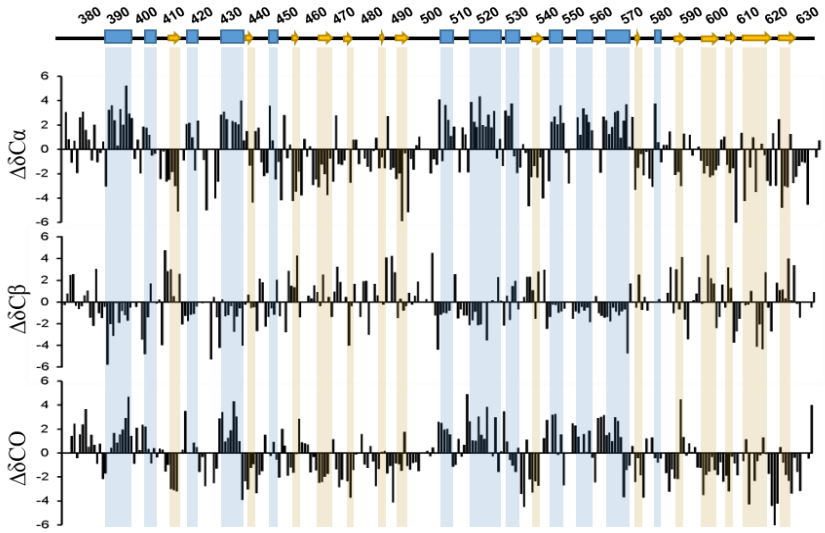

Figure 3. Secondary structure of FAS1-3/FAS1-4 based on the crystal structure and NMR data. upper secondary diagram is represented according to crystal structure (PDB ID 5NV6) and deviations of the observed chemical shift values for backbone ^{13}Cα, ^{13}Cβ and ^{13}CO resonances from corresponding random coil chemical shift values.

Backbone assignment of FAS1-3/FAS1-4 – In this work, FAS1-3/FAS1-4 and FAS1-4 were successfully over-expressed and purified via the protocol described above. ^{1}H-^{15}N HSQC spectrum of FAS1-3/FAS1-4 shows well dispersed amide peaks (7 – 11 ppm), which indicates that FAS1-3/FAS1-4 contains β-strands and is well folded. Furthermore, most of amide peaks could be observed (253 of the 254 expected peaks). Backbone NMR resonances were successfully assigned using standard ^{1}H-^{15}N TROSY-HSQC (Figure 2) and TROSY-based triple-resonances[14]; 93.8 % of backbone chemical shifts were complete for FAS1-3/FAS1-4 (Table 1). FAS1-4 was also successfully assigned by using 3D NMR spectra.

Comparison of the NMR chemical shifts to the crystal structure – Each protein structure determined using solution NMR and crystallography sometimes has different characteristics. Therefore, it was necessary to compare the structural characteristics obtained by solution NMR with those obtained from the existing crystal structure. Due to the lack of 3D solution structure of FAS1-3/FAS1-4 in this work, the comparison of secondary structures was selected as alternative. Secondary structure of FAS1-3/FAS1-4 was defined using chemical shift index (CSI) of Cα, Cβ, CO atoms. In the figure 2, the positive bars of ΔCα and ΔCO, and the negative bars of ΔCβ indicate alpha helix and the negative bars of ΔCα and ΔCO, and the positive bars of ΔCβ indicate beta strand. According to crystal structure, FAS1-3/FAS1-4 contains twelve α helices and fourteen β sheets, which is presented as secondary structure diagram at the top of figure 3. As shown in the figure 3, secondary structure defined using NMR data is relatively well in accordance with that of crystal structure. In other words, NMR data reported in the present work and the crystal structure can be used complementarily.

Structural comparison between FAS1-3/FAS1-4 and FAS1-4 – In this work, both truncated proteins, FAS1-3/FAS1-4 and FAS1-4 were prepared, and well-separated ^{1}H-^{15}N TROSY-HSQC spectra of those were collected. The chemical shifts of amide ^{1}H and ^{15}N can provide useful structural information which is influenced by different factors in their local environment. Especially, ^{1}H-^{15}N HSQC correlation spectrum is frequently used to detection of protein

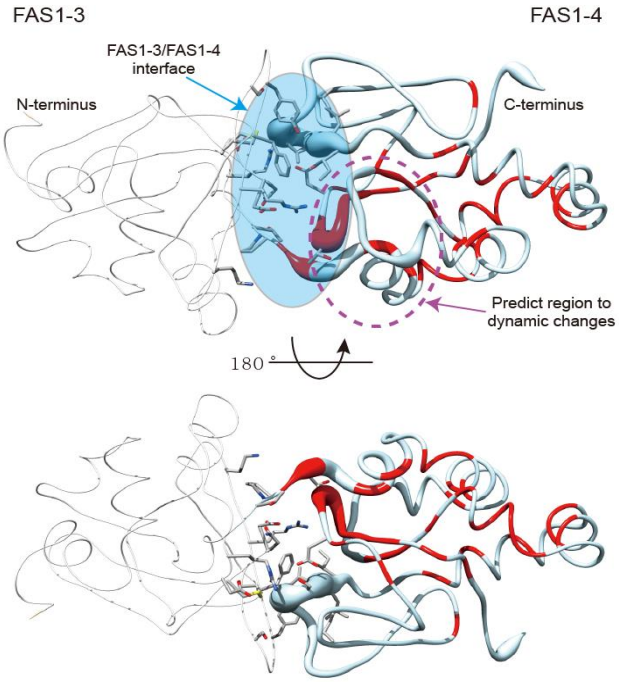

Figure 4. Chemical shift perturbation and disease-related mutations marked on crystal structure of FAS1-3/FAS1-4 (PDB ID 5NV6). Radius and red color represent CSP values calculated from ^{1}H and ^{15}N shifts and disease-related mutation sites, respectively. Circle filled with blue and magenta circle indicate FAS1-3/FAS1-4 interface and dynamic changes-predicted region

folding state and protein-protein(ligand) interaction. For that reason, chemical shift perturbations (CSP) between FAS1-3/FAS1-4 and FAS1-4 were analyzed to understand direct interaction of FAS1-4 with FAS1-3. These perturbations are mapped onto a FAS1-4 structure where CSP values are shown as radius to reveal interaction sites. The result of CSP also shows that the region of structural changes in the FAS1-4 caused by adding FAS1-3 are well match to the interface between FAS1-3 and FAS1-4 in the crystal structure, which is represented in the blue circular region in the figure 4. Interestingly, the residues located in the magenta circle belongs to protein core region that contributes to protein folding and stability in the figure 4, nevertheless, those seem to undergo dynamic changes according to CSP results. In this work, detailed dynamic data was not provided, however, the NMR information would be useful to proceed protein dynamic studies.[15]

TGFBIp-CDs are known to be caused by the aberrant accumulation of proteins possessing mutated residues on the 53 positions reported in the current clinical literature where they are mainly located in FAS1-4 (43 position) colored red on the structure in the figure 4 and FAS1-1 (7 position).[9] 24 of the 43 mutation sites in FAS1-4 and 2 sites in FAS1-3 (not presented in figure 4) are at least partially exposed to surface. The others are located at the inside region. In general, a surface-exposed region is possibly associated to protein-protein or protein-ligand interaction and the core region participates to protein folding or stability.[9, 16] In the same context, the disease-related mutations of FAS1-4 belonging to both region, protein surface and core, affect binding capacities or stability of TGFBIp. Nevertheless, the exact mechanism of mutation sites as well as the reason why those are located on mainly FAS1-1 and FAS1-4 are not clear yet. The NMR assignment data reported here would be essential for further structural studies to answer those questions.

Table 1. Backbone assignments of FAS1-3/FAS1-4

Residue		HN	N	Cα	Cβ	CO
373	P	n.a.	n.d.	n.d.	n.d.	n.d.
374	D	8.76	123.41	57.16	38.97	177.20
375	S	7.82	110.50	59.12	62.42	173.67
376	A	7.71	123.05	51.40	19.80	178.54
377	K	7.95	119.92	57.41	34.81	178.95
378	T	9.05	113.01	61.16	70.68	174.77
379	L	8.33	121.07	58.33	41.55	178.67
380	F	7.92	115.79	60.99	38.63	178.18
381	E	7.60	118.42	58.30	29.30	179.78
382	L	8.32	119.48	56.49	42.50	177.62
383	A	7.44	116.98	51.59	20.07	178.61
384	A	7.56	123.36	54.53	17.55	177.77
385	E	8.38	116.21	55.64	27.48	175.21
386	S	7.54	115.25	58.00	65.74	174.49
387	D	8.58	118.98	54.73	39.74	175.03
388	V	7.84	110.45	59.94	30.22	175.39
389	S	7.50	117.59	61.53	62.25	n.d.
390	T	9.45	124.75	66.71	62.30	175.63
391	A	9.67	125.39	54.90	16.96	178.78
392	I	7.85	115.73	62.91	34.37	177.66
393	D	7.81	120.92	57.42	40.70	178.77
394	L	8.10	121.04	57.72	39.97	179.07
395	F	8.38	116.84	63.12	38.46	178.72
396	R	8.05	118.44	59.25	29.07	181.20
397	Q	9.03	122.27	58.78	28.36	177.74
398	A	8.19	118.21	51.70	18.47	176.21
399	G	7.71	105.64	45.81	n.a.	175.71
400	L	7.96	119.19	53.71	41.44	177.35
401	G	9.13	108.74	46.87	n.a.	175.97
402	N	8.81	119.42	55.39	35.50	177.71
403	H	7.20	115.29	57.00	27.17	175.43
404	L	7.43	116.87	55.18	40.47	176.22
405	S	7.41	111.02	57.93	64.40	174.10
406	G	7.31	112.09	44.98	n.a.	173.24
407	S	8.09	114.67	55.85	62.57	174.06
408	E	7.91	121.54	56.53	29.92	176.37
409	R	8.42	122.49	53.64	26.29	174.94
410	L	6.68	125.16	53.20	46.68	176.11
411	T	8.84	116.53	61.24	70.94	172.20
412	L	8.79	128.18	52.67	44.92	174.00
413	L	9.03	126.79	53.34	39.28	173.57
414	A	8.57	125.00	47.39	19.53	173.90
415	P	n.a.	n.d.	n.d.	n.d.	n.d.
416	L	7.56	120.41	54.80	44.51	177.39
417	N	8.86	118.28	55.70	36.93	179.01
418	S	8.21	114.82	60.46	61.41	n.d.
419	V	7.79	122.68	63.98	29.94	177.10
420	F	7.34	118.05	56.17	38.13	176.66
421	K	7.27	122.06	59.05	31.18	176.99
422	D	8.56	117.68	54.04	40.39	175.61
423	G	7.55	109.04	44.11	n.d.	173.27
424	T	8.11	111.66	58.07	68.00	172.44
425	P	n.a.	n.d.	n.d.	n.d.	n.d.
426	P	n.a.	n.d.	n.d.	n.d.	n.d.
427	I	8.71	121.63	58.56	32.20	174.27
428	D	7.57	127.39	51.43	41.27	175.91
429	A	8.52	120.63	55.35	17.58	180.00
430	H	8.12	118.03	58.89	27.77	178.52
431	T	9.16	120.72	65.58	68.34	176.16
432	R	8.71	122.63	n.d.	28.98	177.79
433	N	7.81	116.77	55.94	37.80	177.41
434	L	8.08	121.89	57.92	41.51	181.43
435	L	8.68	120.94	57.76	39.13	180.15
436	R	8.13	121.15	60.32	28.94	177.49
437	N	7.32	112.73	54.34	38.39	171.59
438	H	7.89	112.96	57.30	27.97	172.74
439	I	7.20	118.44	61.25	37.25	173.75
440	I	9.31	128.93	58.23	38.18	175.55
441	K	8.16	125.05	58.21	31.74	175.58
442	D	7.22	114.60	55.89	40.31	173.85
443	Q	8.48	120.79	55.12	27.42	174.46
444	L	7.54	128.72	53.51	44.06	175.56
445	A	8.06	121.02	50.56	20.82	178.63
446	S	10.50	126.07	61.89	60.44	n.d.
447	K	8.18	119.22	57.43	30.91	176.27
448	Y	7.28	115.64	56.14	38.09	176.63
449	L	7.12	122.42	54.65	40.72	176.54
450	Y	8.10	117.30	54.43	40.74	173.65
451	H	8.71	120.19	58.63	30.68	177.13
452	G	8.53	117.03	44.28	n.a.	174.24
453	Q	7.63	124.75	56.59	27.29	174.41
454	T	7.92	114.11	58.86	70.97	173.99
455	L	9.20	124.36	52.21	43.40	175.46
456	E	8.81	123.40	54.88	31.05	176.00
457	T	8.84	114.11	59.31	72.39	178.07
458	L	8.85	121.42	56.54	40.49	178.01
459	G	7.60	103.84	44.40	n.a.	174.40
460	G	7.80	109.51	45.24	n.a.	174.32
461	K	7.40	119.23	53.77	32.86	174.90
462	K	8.26	120.57	54.22	32.63	176.17
463	L	9.08	123.66	52.58	43.43	175.63
464	R	9.47	123.04	55.06	31.21	174.01
465	V	7.41	119.01	60.95	31.30	174.68
466	F	9.25	128.75	54.15	41.84	173.80
467	V	10.40	126.68	62.25	31.70	175.37
468	Y	8.29	127.14	55.94	39.18	175.63
469	R	8.63	120.08	59.10	28.92	177.66
470	N	8.35	112.49	52.39	39.95	174.12
471	S	7.08	112.11	57.03	65.96	170.83
472	L	8.51	126.05	54.77	43.75	174.85
473	C	9.35	124.13	55.82	49.85	171.00
474	I	9.59	124.77	59.85	37.98	174.45
475	E	8.40	119.56	57.51	25.65	172.38
476	N	8.69	112.46	54.41	38.61	174.08
477	S	8.12	115.69	57.07	64.36	173.57
478	C	8.98	126.47	55.92	46.39	174.05
479	I	8.63	123.52	61.83	36.13	178.38
480	A	9.59	130.65	51.05	20.92	176.13
481	A	7.54	118.86	50.68	20.94	175.85
482	H	8.38	116.84	55.66	28.97	175.70
483	D	8.70	124.19	55.06	40.81	176.48
484	K	8.15	120.77	55.14	33.96	173.72
485	R	8.96	127.56	55.63	30.91	175.17
486	G	8.37	115.37	43.44	n.a.	173.68
487	R	8.01	120.77	59.02	30.06	176.70
488	Y	n.d.	n.d.	56.93	42.82	173.99
489	G	7.65	103.17	43.46	n.a.	172.50
490	T	8.46	117.52	60.66	72.36	171.08
491	L	9.31	127.73	53.70	44.64	176.24
492	F	9.63	131.26	51.99	37.82	174.86
493	T	7.92	121.68	62.75	68.40	173.71
494	M	8.47	125.03	51.43	32.00	177.28
495	D	8.93	117.61	53.30	40.40	176.11
496	R	7.30	112.41	54.62	31.16	175.10
497	V	8.56	123.11	63.35	31.45	176.27
498	L	10.31	134.49	56.75	42.47	176.32
499	T	9.29	115.01	54.16	69.97	173.69
500	P	n.a.	n.d.	n.d.	n.d.	n.d.
501	P	n.a.	n.d.	n.d.	n.d.	n.d.
502	M	8.68	119.25	54.61	33.05	175.69
503	G	7.88	108.65	44.17	n.a.	173.34
504	T	9.56	112.79	61.83	72.65	175.68
505	V	9.76	119.81	67.09	30.46	177.10
506	M	6.84	113.06	55.61	28.37	178.12
507	D	7.49	120.91	57.74	39.61	179.72
508	V	8.10	121.04	65.42	30.70	179.07
509	L	8.01	117.38	56.80	40.87	179.13
510	K	8.45	115.04	58.58	31.49	178.06
511	G	7.45	104.87	44.96	n.a.	172.44
512	D	7.00	120.45	52.19	43.37	176.20
513	N	8.90	125.65	55.40	37.49	176.69
514	R	8.55	119.12	57.53	29.60	176.19
515	F	7.55	113.44	56.00	38.06	176.49
516	S	7.44	116.91	62.19	61.46	178.61

Residue		HN	N	Cα	Cβ	CO
517	M	9.23	124.54	58.88	30.66	178.13
518	L	8.60	124.31	57.54	40.20	178.16
519	V	8.98	119.24	67.35	30.81	178.14
520	A	7.33	122.32	54.50	16.87	180.14
521	A	8.18	123.71	54.38	16.94	178.61
522	I	8.87	120.45	65.44	37.45	177.98
523	Q	7.75	119.32	58.02	26.54	180.17
524	S	8.30	118.50	61.45	62.74	n.a.
525	A	8.22	119.45	51.75	19.16	176.81
526	G	7.71	106.16	45.85	n.a.	176.58
527	L	8.06	118.99	54.34	44.19	175.52
528	T	7.50	118.47	66.28	68.22	175.37
529	E	8.24	117.97	59.45	27.53	179.59
530	T	7.75	116.33	66.86	68.66	176.17
531	L	7.09	116.34	55.13	40.23	176.50
532	N	7.85	121.33	51.65	40.47	174.45
533	R	7.15	120.25	54.81	32.25	174.92
534	E	8.43	119.45	57.14	28.99	176.54
535	G	8.07	111.08	44.69	n.a.	170.19
536	V	7.03	114.55	58.32	32.18	172.59
537	Y	7.13	117.29	56.31	41.04	176.83
538	T	7.77	117.22	61.72	70.44	172.99
539	V	9.23	127.54	60.67	32.79	173.80
540	F	9.01	128.82	57.22	37.73	173.43
541	A	8.53	126.25	48.46	21.80	174.38
542	P	n.a.	n.d.	n.d.	n.d.	n.d.
543	T	7.75	112.29	60.47	71.07	176.43
544	N	8.84	119.23	55.86	36.51	178.28
545	E	8.21	118.84	59.39	28.33	n.a.
546	A	7.40	122.11	54.57	18.76	180.30
547	F	7.22	115.31	61.51	39.00	179.07
548	R	8.21	118.84	58.46	29.29	176.35
549	A	7.33	119.07	52.21	18.12	178.65
550	L	7.04	119.87	52.90	41.27	174.39
551	P	n.a.	n.d.	n.d.	n.d.	n.d.
552	P	n.a.	n.d.	n.d.	n.d.	n.d.
553	R	8.89	117.34	58.94	28.73	178.99
554	E	7.48	120.02	57.89	28.83	178.39
555	R	8.45	120.61	59.67	29.27	177.88
556	S	8.12	112.17	61.15	62.26	n.a.
557	R	7.52	122.72	58.53	29.49	178.09
558	L	7.97	118.19	57.27	41.37	177.18
559	L	7.74	112.15	55.69	40.02	178.95
560	G	7.50	104.94	45.02	n.d.	173.20
561	D	7.22	121.13	52.17	41.35	174.75
562	A	8.61	127.17	55.20	17.95	180.02
563	K	8.07	118.61	59.07	31.02	179.53
564	E	7.78	121.99	57.95	28.26	179.29
565	L	8.71	121.05	57.54	40.52	178.60
566	A	7.99	119.17	55.56	17.22	178.81
567	N	7.38	115.72	56.75	38.49	176.49
568	I	8.01	117.13	63.54	36.61	179.80
569	L	8.97	121.29	58.05	40.65	179.78
570	K	8.49	116.71	60.42	31.43	177.83
571	Y	7.57	120.14	58.80	38.01	171.99
572	H	7.44	109.39	58.45	27.26	173.66
573	I	7.22	118.04	59.27	39.20	175.73
574	G	10.25	112.00	43.47	n.a.	174.20
575	D	8.30	120.49	53.72	40.27	174.79
576	E	7.27	114.73	54.57	32.24	175.67
577	I	8.12	119.66	62.39	36.78	174.92
578	L	8.30	137.00	53.29	42.37	173.37
579	V	6.78	117.72	59.91	30.89	178.33
580	S	11.44	123.36	62.05	n.d.	n.d.
581	G	9.51	110.52	45.58	n.a.	174.92
582	G	8.00	108.55	43.94	n.a.	173.17
583	I	6.92	121.25	62.98	37.75	176.00
584	G	7.98	111.22	45.38	n.a.	173.15
585	A	8.21	126.04	53.97	18.97	177.17
586	L	7.75	119.25	55.69	42.76	175.41
587	V	9.49	128.32	60.89	34.92	173.85
588	R	8.55	125.37	54.45	29.26	175.13
589	L	8.79	127.98	52.67	44.92	174.97
590	K	9.42	129.48	58.00	31.61	174.31
591	S	7.85	121.33	n.d.	66.86	178.17
592	L	9.22	121.61	56.90	40.26	178.43
593	Q	7.51	119.36	55.68	26.64	176.10
594	G	7.56	109.66	45.02	n.a.	174.40
595	D	8.87	121.03	54.32	40.98	177.29
596	K	9.10	119.25	55.76	33.08	176.99
597	L	9.37	126.58	53.71	44.18	175.90
598	E	8.28	121.53	55.32	29.53	174.85
599	V	9.24	131.12	60.70	31.72	173.57
600	S	9.06	120.41	56.15	67.02	171.86
601	L	7.75	122.93	53.98	44.09	175.54
602	K	8.25	126.87	55.35	34.01	176.16
603	N	9.52	127.23	54.39	36.58	174.08
604	N	8.60	109.12	54.64	37.62	173.68
605	V	7.83	122.02	61.72	33.32	176.32
606	V	9.39	133.86	61.05	31.17	174.72
607	S	9.01	120.78	56.74	65.90	171.79
608	V	9.13	121.35	56.92	32.99	173.89
609	N	9.70	128.48	53.50	35.24	175.19
610	K	8.18	107.37	58.06	29.59	175.62
611	E	8.47	125.32	52.44	28.13	174.24
612	P	n.a.	n.d.	n.d.	n.d.	n.d.
613	V	9.13	125.15	61.49	31.38	176.41
614	A	8.85	132.71	53.49	18.73	178.25
615	E	6.77	115.30	53.18	30.73	171.82
616	P	n.a.	n.d.	n.d.	n.d.	n.d.
617	D	9.63	114.30	54.55	36.68	174.86
618	I	8.78	120.96	62.10	35.44	176.11
619	M	8.16	125.30	54.01	28.42	175.31
620	A	8.79	123.14	49.49	21.74	178.40
621	T	9.64	114.85	64.40	67.57	175.10
622	N	8.07	115.87	50.61	36.27	173.75
623	G	7.12	102.28	47.47	n.a.	169.17
624	V	8.40	119.56	58.21	33.49	170.57
625	V	9.07	128.62	59.97	32.79	172.85
626	H	8.65	124.47	52.68	33.17	175.61
627	V	8.82	125.19	64.26	32.05	176.29
628	I	8.57	121.34	59.83	41.50	174.98
629	T	9.30	108.89	60.85	68.26	172.88
630	N	7.31	118.02	52.23	42.40	172.11
631	V	8.11	118.57	61.95	31.50	176.70
632	L	10.75	131.83	54.60	40.44	175.52
633	Q	7.78	115.85	51.66	30.14	173.12
634	P	n.a.	n.d.	n.d.	n.d.	n.d.
635	P	n.a.	n.d.	n.d.	n.d.	n.d.
636	A	8.23	125.21	51.83	18.48	176.62
637	N	7.86	123.69	54.33	39.92	179.50

Acknowledgements

This work was supported by the research grant of the Chungbuk National University in 2017 and NRF-2019R1F1A1057427. The use of NMR was supported by the Korea Basic Science Institute under the R&D program (Project No. D39701) supervised by the Ministry of Science and ICT.

References

1. J. Skonier, M. Neubauer, L. Madisen, K. Bennett, G. D. Plowman, and A. F. Purchio, *DNA Cell Biol.* **11**, 511 (1992)
2. J. Escribano, N. Hernando, S. Ghosh, J. Crabb, and M. Coca-Prados, *J. Cell Physiol.* **160**, 511 (1994)
3. R. Lakshminarayanan, S. S. Chaurasia, E. Murugan, A. Venkatraman, S. M. Chai, E. N. Vithana, R. W. Beuerman, and J. S. Mehta, *Ocul. Surf.* **13**, 9 (2015)
4. K. E. Han, S. I. Choi, T. I. Kim, Y. S. Maeng, R. D. Stulting, Y. W. Ji, and E. K. Kim, *Prog. Retin. Eye Res.* **50**, 67 (2016)
5. R. B. Andersen, H. Karring, T. Moller-Pedersen, Z. Valnickova, I. B. Thogersen, C. J. Hedegaard, T. Kristensen, G. K. Klintworth, and J. J. Enghild, *Biochemistry* **43**, 16374 (2004)
6. J. S. Weiss, H. U. Moller, A. J. Aldave, B. Seitz, C. Bredrup, T. Kivela, F. L. Munier, C. J. Rapuano, K. K. Nischal, E. K. Kim, J. Sutphin, M. Busin, A. Labbe, K. R. Kenyon, S. Kinoshita, and W. Lisch, *Cornea* **34**, 117 (2015)
7. N. Thapa, B. H. Lee, and I. S. Kim, *Int. J. Biochem. Cell Biol.* **39**, 2183 (2007)
8. J. Skonier, K. Bennett, V. Rothwell, S. Kosowski, G. Plowman, P. Wallace, S. Edelhoff, C. Disteche, M. Neubauer, and H. Marquardt, *DNA Cell Biol.* **13**, 571 (1994)
9. C. Kannabiran and G. K. Klintworth, *Hum. Mutat.* **27**, 615 (2006)
10. R. V. Basaiawmoit, C. L. Oliveira, K. Runager, C. S. Sorensen, M. A. Behrens, B. H. Jonsson, T. Kristensen, G. K. Klintworth, J. J. Enghild, J. S. Pedersen, and D. E. Otzen, *J. Mol. Biol.* **408**, 503 (2011)
11. J. Underhaug, H. Koldso, K. Runager, J. T. Nielsen, C. S. Sorensen, T. Kristensen, D. E. Otzen, H. Karring, A. Malmendal, B. Schiott, J. J. Enghild, and N. C. Nielsen, *Biochim. Biophys. Acta* **1834**, 2812 (2013)
12. J. H. Yoo, E. Kim, J. Kim, and H. S. Cho, *Acta Crystallogr. Sect. F Struct. Biol. Cryst. Commun.* **63**, 893 (2007)
13. R. Garcia-Castellanos, N. S. Nielsen, K. Runager, I. B. Thogersen, M. V. Lukassen, E. T. Poulsen, T. Goulas, J. J. Enghild, and F. X. Gomis-Ruth, *Structure* **25**, 1740 (2017)
14. K.-S. Jo, D.-W. Sim, E.-H. Kim, D.-H. Kim, Y.-B. Ma, J.-H. Kim, and H.-S. Won, *J. Kor. Magn. Reson. Soc.* **22**, 64 (2018)
15. S. Yoo and C.-J Park, *J. Kor. Magn. Reson. Soc.* **22**, 18 (2018)
16. K. Runager, R. V. Basaiawmoit, T. Deva, M. Andreasen, Z. Valnickova, C. S. Sorensen, H. Karring, I. B. Thogersen, G. Christiansen, J. Underhaug, T. Kristensen, N. C. Nielsen, G. K. Klintworth, D. E. Otzen, and J. J. Enghild, *J. Biol. Chem.* **286**, 4951 (2011)